International Journal of Adhesion & Adhesives 57 (2015) 13–21

Contents lists available at ScienceDirect

International Journal of Adhesion & Adhesives

journal homepage: www.elsevier.com/locate/ijadhadh

Bond characterization of adhesively bonded joints made with the resin infusion (RI) process

S.A. Hadigheh [a,*], R.J. Gravina [a], S. Setunge [a], S.J. Kim [b]

[a] School of Civil, Environmental and Chemical Engineering, RMIT University, Melbourne, VIC 3001, Australia
[b] Wagners CFT, Queensland, Australia

ARTICLE INFO

Article history:
Accepted 2 August 2014
Available online 13 October 2014

Keywords:
Resin infusion
FRP
Concrete
Modified single lap shear test
Thickness
Bond

ABSTRACT

In this research, the bond characteristics between concrete and FRP plates processed with resin infusion technique are studied. The bondline thickness is varied and a new modified single lap shear (MSLS) test set-up is implemented to monitor the interface during the experiments. Based on MSLS test set-up, the relative displacement between FRP adherend and substrate can be monitored with higher precision. Nonlinear analysis of the MSLS test results indicates that the maximum applied load increases for thicker bondline until a certain amount of thickness, optimum bondline thickness, beyond which no increase in load is achieved. Therefore, a relationship is proposed to estimate the maximum applied load based on bondline thickness. In addition, the interfacial performance of RI processed plates is also compared with the pultruded laminates bonded to the concrete. Results show that the samples processed by RI technique follow the same debonding mechanism as the pultruded specimens.

1. Introduction

The repair of concrete structures via bond of fibre reinforced polymer (FRP) materials onto the substrate has been extensively carried out by two commonly used methods, pultruded laminates or wet lay-up (or hand lay-up) systems. In the pultruded plate repair system, prefabricated plates are bonded to the substrate by epoxy adhesives. The wet lay-up method involves the impregnation of unidirectional or weaved fibres by a low-viscosity epoxy adhesive using rollers or brushes. However, with the wide application of the composite materials in the strengthening of infrastructures, new processing techniques with higher quality are necessary to achieve the reliable FRP repairing systems.

Resin infusion (RI) and resin transfer moulding (RTM) have been used in marine, petroleum and composite manufacturing industries in a large scale to reduce production cost, make complex geometry with large components, produce composites with high fibre volume fraction and to improve the quality of the products [1]. As well as marine industry [2–4], RI and RTM techniques have been used widely in other fields such as aerospace for production of light weight profiles with low operation cost and increase of the payload [5]. From material science and manufacturing point of view, several investigations have been carried out to study the efficiency of the resin injection method or resin transfer moulding compared with other commonly used processing techniques [6–10].

In RI and RTM, the reinforcement is placed on a rigid mould and covered with a layer of the peel ply and the flow medium. The whole system is isolated by another rigid mould while the vacuum is induced into the system. The vacuum distributes the resin over and inside of the reinforcement. Using the vacuum results in the production of the components with better mechanical properties, lower porosity levels and accurate fibre management [11,12]. The flow of the resin will be improved using higher permeable flow medium both in the plane and transverse directions. The resin spreads along the flow medium plane and then penetrates downward into the prefabricated fibres. Therefore, a 3D model is required to simulate the resin infusion process. Since the thickness of composite is very small compared with other dimensions therefore, the resin flow in the thickness direction is negligible [13] and the flow model is called 2½ dimensional. It was shown [1] that flow path along the transverse direction follows a parabolic profile.

In resin transfer moulding, the mould consists of two rigid parts while the resin infusion is sealed with one rigid mould and a vacuum bag [14,15]. The advantage of using flexible vacuum bag in RI (also known as resin infusion under flexible tooling, RIFT) system facilitates to make complex profiles with low cost. The vacuum bag is fixed to the mould using vacuum sealant tapes around the bag. In RI process, the resin application is under control and transferred from the resin reservoir through the injection units and finally into the mould using vacuum forces. Therefore, the chemical emission and contact with the composite will be

* Corresponding author. Tel.: +61 3 9925 1709.
E-mail address: seyedali.hadigheh@rmit.edu.au (S.A. Hadigheh).

http://dx.doi.org/10.1016/j.ijadhadh.2014.10.001
0143-7496/

minimized in the RI process compared with wet lay-up and pultruded laminate techniques.

Although the use of RI system is common in marine and aerospace industries, very less attention has been paid to the application of this system in the strengthening of structures using FRP materials. Since the resin infusion process can be applied to large components with high mechanical properties and low cost [16,17], it is suitable for structural strengthening of infrastructures. The successful application of the vacuum-injection system in shear strengthening of the reinforced concrete beams is compared with the hand lay-up method [18]. Results showed that the strength of the fractured beams can be restored to the same amount in uncracked beams [18].

The vacuum bag curing was applied to bond the concrete to the shuttering in composite beams, consisted of fibre reinforced polymer materials and concrete [19]. The resin injection method was able to satisfy the level of composite action in the composite beams. In addition, the vacuum resin infusion is used in fabrication of FRP bridges for replacement of the deteriorated structures (e.g. Bennett's Creek in US [20] and West Mill Bridge in Oxfordshire, UK). The significant strength was achieved for the replaced bridges which is reported after prototype and field proof tests with the application of a full-scale load. The strengthening was carried out with less construction time and cost effectiveness [21,22]. In addition, the successful application of the resin infusion system in concrete-filled FRP tubes in strengthening of the bridge structures [23] and enhancement of the punching resistance of GFRP composite sandwich panels [24] has been reported.

2. Research significance and objectives

Various researches have been undertaken to investigate the bond behaviour between concrete and the FRP considering commonly used processing techniques such as, wet lay-up or pultruded systems. These studies mainly address the effects of different parameters on the bond performance via experimental, analytical and/or the numerical approaches. Nevertheless, the influence of the application of different FRP manufacturing methods has received less consideration in the interface study. Among wet lay-up, pultruded and RI processing techniques, the available experimental data about the bond characteristics between concrete and the resin infusion is limited.

Therefore, the interfacial behaviour between concrete and FRP plates, processed by the resin infusion technique, is investigated in this article. Single lap shear tests are performed on several adhesively bonded joints using a modified test set-up, proposed and successfully tested by the authors [25,26]. In addition, the bondline thickness of samples is varied between 2 and 6 mm in the experiments. The current research provides an experimental database regarding the interface behaviour between concrete and RI processed FRP plates with the focus on the bondline thickness. In addition, the bond performance between concrete substrate and the FRP is compared for samples which are manufactured by RI and pultrusion methods.

3. RI application technique

Prior to the application of RI technique, the surface of the sample should be cleaned to avoid any deficiency inside of the bond between substrate and the FRP plates. The dry plate preform is placed on the mould (here, concrete) and fixed by applying the spray adhesive. Subsequently, the peel ply and the flow medium are placed on the plates. The flow (infusion) medium is used to aid the resin to be distributed and spread over the bond area. To take off the disposable parts, a peel ply layer is arranged between the flow medium and the vacuum bag. Then, the whole system is covered by a specific plastic bag in order to produce the vacuum condition during the RI technique. The vacuum bag can be sealed all around by the vacuum sealant tapes (the double sticking tape). The inlet and outlet tubes are located at the start and the end point of the mould to supply resin and remove the air, respectively. The inlet tube is attached to the resin hose (or resin tank) and the outlet tube is connected to the vacuum hose (or vacuum pump).

The vacuum pulls the resin down through the flow medium, plate preform and the interface between the FRP and the mould (substrate). Therefore, the epoxy can fast saturate the dry fibres and bond them together as well as to the substrate. When the resin covers all the area, the inlet tube (resin supply) is closed and the bonded area is kept under the vacuum condition until the resin is cured under ambient temperature. The excessive resin is trapped in a resin trap tank before it flows to the vacuum pump. A schematic view of the resin infusion is shown in Fig. 1.

The presence of the vacuum minimizes the formation of dry spot areas on the cured FRP which leads to higher quality of the composite. Therefore, the vacuum pressure has an important role on the performance of the RI system. Although 78—98 kPa pressure is reasonable to produce the vacuum, it depends on the substrate porosity, higher vacuum pressure is necessary. If sufficient pressure is not used, the composite may be of low fibre volume fraction with some unsaturated spots on the plates [5].

4. Test methodology and materials

4.1. Specimen fabrication and material characterization

In this section, the experimental programme to investigate the FRP-to-concrete bonded joints is described. The modified single lap shear (MSLS) test is conducted on the concrete prisms pre-

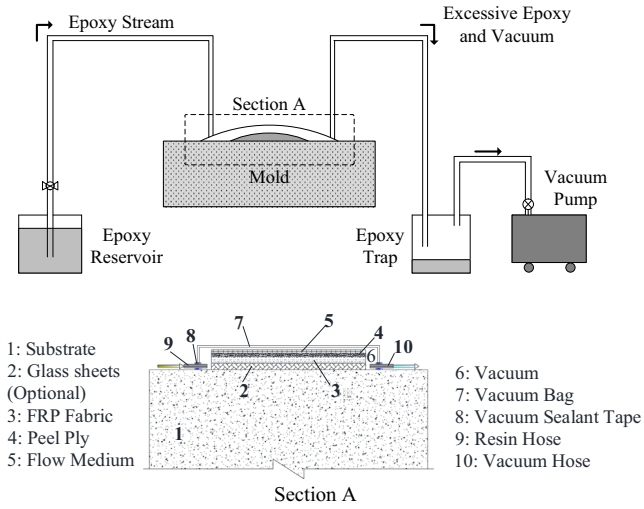

Fig. 1. RI application process.

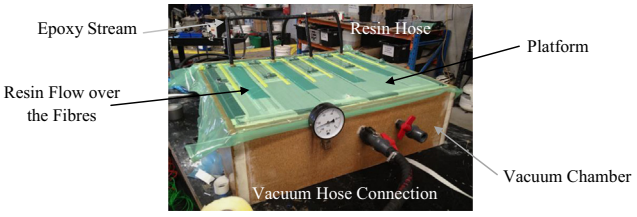

Fig. 2. Application of RI on the concrete specimens.

attached with CFRP plates using resin infusion system. A platform with the vacuum chamber was made to keep four concrete specimens tightly in position while the FRP was processed with RI system (Fig. 2). The platform also helped to attain better quality of the interface in the bonded region. The inside space of the vacuum chamber was isolated from the outside by the vacuum bag and sealant tapes installed around the chamber. The resin was transferred from the epoxy reservoir to the fibres by four resin hoses. The vacuum provided a force to propagate the epoxy over the carbon fibres. When the epoxy completely saturated the fibres, the valve on the resin hose was shut to maintain the vacuum pressure during the curing time. The samples were kept under vacuum for almost 24 h while the epoxy was cured. The process of RI is described in detail in Section 3.

Concrete blocks and standard cylinders were made of normal Portland cement and crushed aggregates with maximum size of 14 mm. The concrete blocks have the dimensions of $150 \times 150 \times 300$ mm^3 (height × width × length). Both cylinders and blocks were cured for 28 days under plastic sheets to avoid cracking on the concrete surface. After 28 day, curing was stopped and standard concrete cylinders were tested under compression, based on ASTM C39/C39M-09a [27], to determine the compressive strength of the concrete at the day of 28 and SLS test. The mean compressive strength of the concrete is presented in Table 1. The average slump value of the concrete was around 80 mm. The gap between concrete casting and SLS test was about 5 months. It allowed that concrete achieved its peak strength, f'_c. Before bonding the fibres on the concrete, blocks were treated by a low pressure (13.8 MPa) water jet blasting. The surface preparation was performed in order to remove the mortar under the bonded region and to expose the aggregates.

Four different bondline thicknesses, from 2 mm to 6 mm, were tested during the experimental programme. For each bondline thickness, three similar specimens were tested to achieve more reliable results. The thickness variation was achieved using RI technique in which the FRP attaching is under control. To increase the thickness, bi-directional GFRP dry fabrics were placed between the substrate and carbon sheets. To minimize the contribution of GFRP layers in load carrying capacity, the GFRP sheets were placed ± 45 degree relative to the direction of the carbon fibres and the applied load. In addition, the glass fibres were cut about 20 mm prior to loaded face of the concrete blocks (Fig. 3). Thickness of each GFRP ply was constant throughout the experiments. However, the number of plies varies from 0 to 6. Tensile modulus of elasticity, E_{gfib}, and tensile strength, T_{gfib}, of the glass fibres are 73 GPa and 3400 MPa, respectively.

Three plies of unidirectional carbon fibres were placed, parallel to the direction of the applied load, on top of the GFRP sheets to make composite plates. Thickness of each carbon ply is 0.337 mm. Modulus of elasticity, E_{cfrp}, and tensile strength, T_{cfrp}, of the carbon plates processed by RI technique are 225 MPa and 2000 MPa, respectively, which are determined based on ASTM D3039-08 [28]. Modulus of elasticity, E_{cfib}, and tensile strength, T_{cfib}, of the carbon fibres before processing are 230 GPa and 4900 MPa, respectively. Fibre areal weight of carbon sheets is 610 g/m^2.

A turane (thermosetting urethane) resin which during curing combines the chemistry of radical polymerization with polyurethane was used to saturate the fibres. Based on the data provided by manufacturer, tensile strength and elastic modulus of the resin were 90 MPa and 3100 MPa, respectively. The FRP width and length adopted for all of the samples were 50 mm and 200 mm, respectively. A 25 mm initial unbonded region was considered between the FRP and concrete to avoid concrete crushing at the loaded end of the concrete blocks. This gap was suggested from the previous research of the authors [29].

4.2. Experimental procedure

A modified single lap shear (MSLS) test set-up (Fig. 4) was installed and employed to determine the interfacial bond characteristics. Using the MSLS test, the slip between the FRP and concrete is measured directly from the start point of the bonded length by means of mounting a LVDT holder on the sides of the concrete [30]. This arrangement contributes to eliminate the errors in slip readings from two LVDTs. However, the movement of the concrete block was monitored during the tests to make sure that the whole system does not experience excessive movements. The front rod was omitted from test set-up in these series of tests to avoid any rotation of the concrete block around the reaction frame. Samples were subjected to a preload of 8 kN followed by a monotonic load at a rate of 0.2 mm/min until failure.

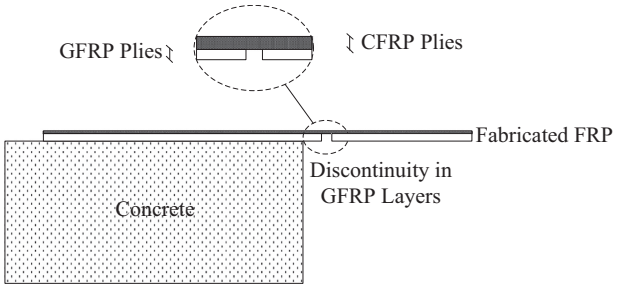

Fig. 3. Configuration of FRP plies to minimize the contribution of GFRP layers in load carrying capacity.

Table 1
Test matrix and specimen properties.

Specimen ID	28th day concrete compressive strength, $f'_{cm,28}$ (MPa)	SLS day concrete compressive strength, $f'_{cm,SLS}$ (MPa)	FRP length, L_{frp} (mm)	FRP width, W_{frp} (mm)	No. of GFRP layers	Bondline thickness, t_{bl} (mm)	Ave. bondline thickness, $t_{bl,ave}$ (mm)
SF-B-1.1	36.5	42.4	200	50	0	2.11	2.01
SF-B-1.2	36.5	42.4				1.91	
SF-B-1.3	–	39.0				2.00	
SF-B-2.1	36.5	42.4	200	50	1	2.49	2.57
SF-B-2.2	–	39.0				2.74	
SF-B-2.3	–	39.0				2.53	
SF-B-2.4	–	39.0				2.50	
SF-B-3.1	36.5	42.4	200	50	3	4.06	3.97
SF-B-3.2	36.5	42.4				4.02	
SF-B-3.3	36.5	42.4				3.82	
SF-B-4.1	36.5	42.4	200	50	6	6.28	6.33
SF-B-4.2	36.5	42.4				6.38	

To investigate the interfacial stresses, six 10 mm-length strain gauges were attached on the surface of the FRP plates. The gauge factor, gauge resistance and temperature compensation for strain gauges were 2.09 ± 1%, 119.5 ± 0.5 Ω and 11 × 10^6/°C, respectively. The first gauge was installed on the FRP at the loaded end and the others were attached with 15, 15, 30, 30 and 40 mm distances from each other toward the free end of the plate. The data from the test set-up was collected by a data logger which is specifically prepared for this research.

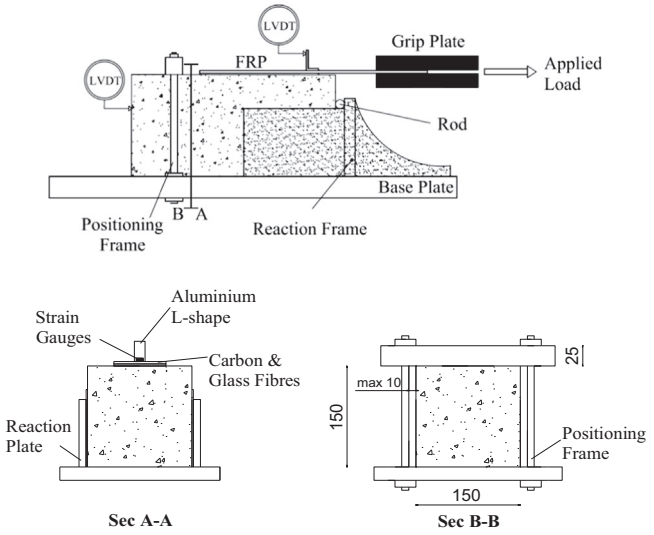

Fig. 4. MSLS test set-up and instrumentation.

5. MSLS test outcomes and discussion

Fig. 5 shows the relation between the load and the global slip of the bonded joints with different bondline thicknesses. The bondline thickness in this study consists of the total thickness of the fibres (glass and carbon) and the adhesive

$$t_{bl} = t_{cfib} + t_{gfib} + t_{adh} \quad (1)$$

where t_{cfib}, t_{gfib}, and t_{adh} are carbon fibre, glass fibre and the adhesive thicknesses, respectively. t_{bl} which is shown in Fig. 5 is the average value of the bondline thicknesses of three identical samples in each group. The global slip is the relative displacement of the FRP plate to the substrate at the loaded end and is monitored by the modified single lap shear test set-up. According to this figure, the load–slip behaviour for the samples follows a similar pattern. During the tests, sample SF-B-2.3 failed prior to reach the ultimate load carrying capacity in the SLS test and is not presented in this article.

Based on efficiency (Krenchel) factor in composites [31], the effect of fibre orientation on stiffness can be determined by the following equation:

$$E_{frp} = \eta_\theta E_f V_f + E_m V_m \quad (2)$$

where η_θ is composite efficiency factor (Krenchel) which is 0.25 for the fibres in ± 45 degree. E and V are modulus of elasticity and volume fraction, while f and m represent fibre and matrix, respectively. Since elasticity modulus of the matrix is remarkably lower than the fibre, the above equation can be expressed as

$$E_{frp} = \eta_\theta E_f V_f \quad (3)$$

Since GFRP sheets are placed between substrate and CFRP fabrics in order to increase the bondline thickness, modulus of

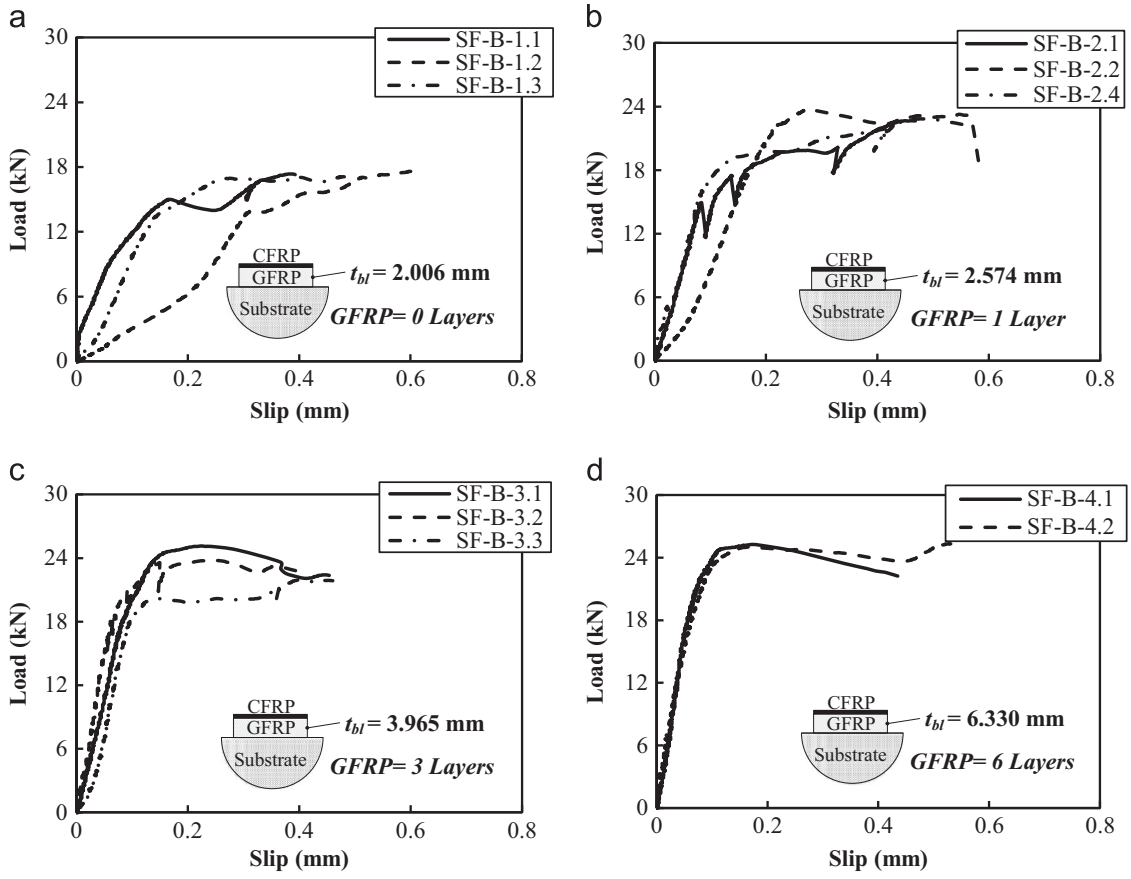

Fig. 5. Load vs slip curve for the samples with (a) 0 GFRP layers, (b) 1 GFRP layer, (c) 3 GFRP layers and (d) 6 GFRP layers.

elasticity of the composite can be determined as

$$E_{frp} = \eta_\theta E_{cf} V_{cf} + \eta'_\theta E_{gf} V_{gf} \quad (4)$$

where E_{cf} and E_{gf} are elastic modulus of carbon and glass fibres, respectively. Considering that the glass fibres are placed ± 45 degree relative to the carbon fibre direction, the contribution of the glass sheets (e.g. for the samples with 6 GFRP layers) in elasticity modulus of the fabricated FRP is

$$0.25 \times 6/9 \times 0.3E_{cf} = 0.05 \quad (5)$$

It is assumed that elastic modulus of the glass fibres is $0.3E_{cf}$ (73/230 GPa/GPa). Therefore, the contribution of the glass fibres is totally about 5 per cent.

The same behaviour (load–slip) is observed for pultruded and heated vacuum bag only (HVBO) samples. In pulruded [26] and HVBO [32] samples, epoxy resins and film adhesives were used, respectively, to increase the bondline. Results showed that the load–slip response of the joints followed the same trend as resin infused (RI) samples. In addition, considering that the GFRP layers are not continues (Fig. 3), it can be concluded that the effect of the GFRP layers on the interface behaviour is negligible.

Considering the load–slip curve of three samples in each group, the initial slope of the samples (linear stage) follows the same trend (Fig. 5c and d). However, for the samples with 0 and 1 GFRP layers, SF-B-1.2 (Fig. 5a) and SF-B-2.2 (Fig. 5b) specimens show different patterns in terms of the initial stiffness. Nevertheless after the maximum load, the behaviour turns out to be quite similar for all of the samples. This response is different for SF-B-3 and 4 groups (Fig. 5c and d). As the bondline thickness increases in SF-B-3 and 4 groups, the specimens show the same initial stiffness.

It was shown that the surface preparation has great influence on the load–slip curve pattern in the SLS tests [29]. Hadigheh et al. [29] reported that the surface preparation may lead to a different initial stiffness in the load–slip curves. Therefore, the distinctive response of SF-B-1.2 and SF-B-2.2, during the initial stage, may attribute to the surface preparation effect. In samples of SF-B-3 and 4 groups, thicker bondline is applied and the effect of the concrete surface is negligible. In addition considering Fig. 8, the depth of cohesive failure, which occurs in a thin layer of concrete substrate, is more for specimens with thicker bondline. Therefore, when the bondline thickness decreases (i.e. in SF-B-1 and 2 groups), the effect of the concrete surface condition on the interfacial behaviour increases.

The total load–slip response of the bonded joints can be categorized into three different stages. During the first stage, increase in the load is accompanied with a small increase in the global slip. Load–slip curves show almost linear behaviour with the maximum slip of 0.07–0.1 mm. After this phase, since the micro-cracks form in the interface between concrete and FRP, the response becomes nonlinear until the propagation of a macro-crack. The slip corresponding to the maximum applied load is between 0.2 and 0.6 mm (Table 2). The nonlinearity of the bond continues until the macro-crack occurs at the interface and the slip increases rapidly while the load carrying capacity remains constant. The ultimate slip varies between 0.4 and 0.6 mm for samples with different thicknesses. Finally when the macro-crack propagates to a certain length, debonding occurs at the interface with an explosive sound. According to the MSLS test results, the maximum global slip at the loaded end, S_{max}, is less than 0.6 mm. This small value could properly be captured by the data taker considering the modified test set-up, which was adopted in this research.

A comparison was made between the load–slip curves of the samples with different bondline thicknesses (Fig. 6). Samples with no and one glass fibre (i.e. samples in group SF-B-1 and SF-B-2) show a soft behaviour during the initial steps of the loading. Since one of the major purposes in the strengthening of the concrete members is binding the emerged cracks on the substrate and preventing them from further growth, the higher the initial stiffness of the strengthening method, the better. Therefore, the samples with no and one GFRP layer cannot sufficiently lock the cracks during the loading while the other samples with 3 and 6 layers of GFRP have quite higher initial stiffness.

Fig. 7 shows the correlation between the average bondline thickness and the maximum applied load for the samples processed with the resin infusion. The curve was fitted to the results of MSLS tests by a nonlinear regression analysis. By increasing the bondline thickness, the maximum applied load increases from 17 kN for t_{bl}=2.01 mm up to 24 kN for t_{bl}=2.57 mm (Table 2).

Table 2
Modified single lap shear test results.

Specimen ID	Experimental max. load, $(F_{max})_{exp.}$, (kN)	Ultimate load, F_u, (kN)	Slip at max. load, S_{max}, (mm)	Ultimate slip, S_u, (mm)	Experimental interfacial fracture energy, $(G_F)_{exp.}$, (N/mm)
SF-B-1.1	17.4	17.3	0.38	0.39	
SF-B-1.2	17.7	17.6	0.60	0.61	
SF-B-1.3	17.1	17.1	0.49	0.49	0.2
SF-B-2.1	22.7	22.6	0.45	0.47	
SF-B-2.2	23.7	18.3	0.27	0.58	
SF-B-2.4	22.8	22.2	0.48	0.56	
SF-B-3.1	25.1	22.4	0.22	0.45	
SF-B-3.2	23.8	22.6	0.24	0.41	
SF-B-3.3	21.9	21.9	0.40	0.46	0.5
SF-B-4.1	25.3	22.2	0.17	0.44	
SF-B-4.2	25.4	25.3	0.53	0.53	0.4

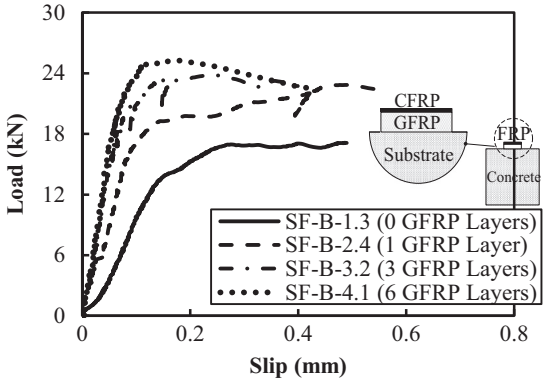

Fig. 6. Comparison between load vs slip curves of the samples with different bondline thicknesses.

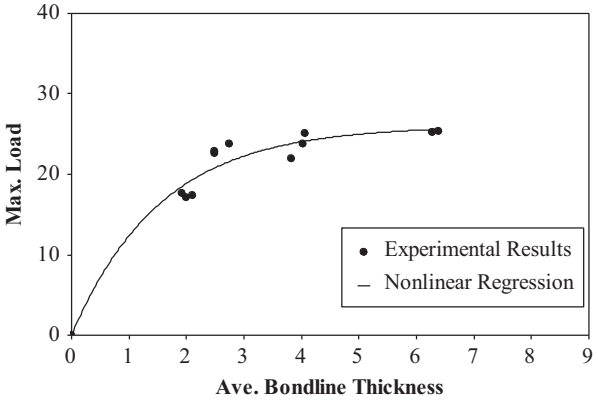

Fig. 7. Relationship between the maximum load and the bondline thickness for the samples processed by RI technique.

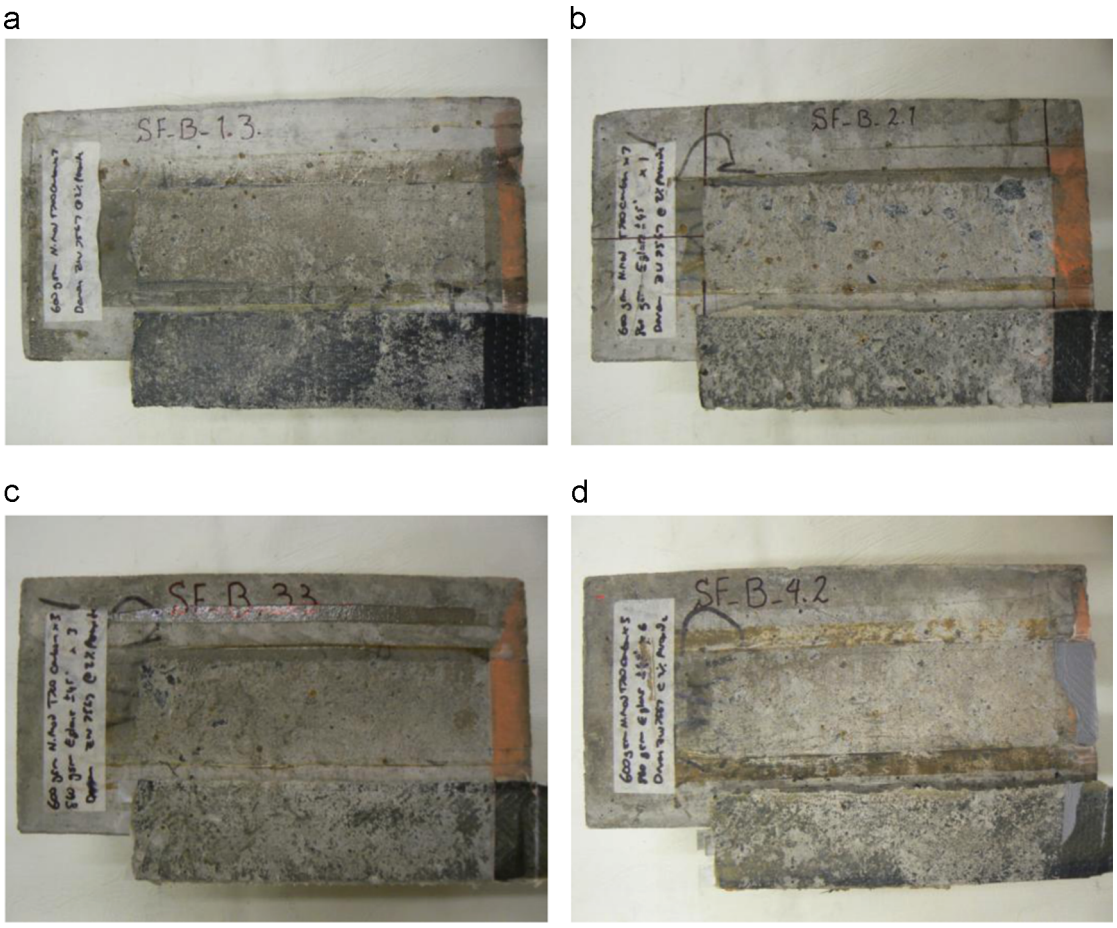

Fig. 8. Fractured interface of the specimens with, (a) 0 GFRP layers, (b) 1 GFRP layer, (c) 3 GFRP layers and (d) 6 GFRP layers.

After this thickness, the load tends to remain constant and any increase in the thickness does not change the maximum load carrying capacity (i.e. samples with 3 or 6 layers of glass fibres). It indicates that the increase in the bondline thickness may not continuously lead to the load carrying capacity enhancement. According to the MSLS tests carried out by the authors, similar behaviour was observed for the pultruded samples and also specimens processed by the heat and vacuum [25,26,32–34].

In the existing empirical and fracture mechanics models, thicker bondline leads to higher load carrying capacity of the joints. However, based on the results of the MSLS tests on the pultruded samples [26] and specimens processed by the heat and vacuum [25,32,34] and also the results of this research, there exists an optimum bondline thickness beyond which no increase in the load can be achieved. This optimum thickness is necessary to be considered in design of the members externally bonded with FRP materials. Therefore, the current formulae for determination of the maximum load need to be verified in order to consider the effect of thickness on the bond behaviour. In this study, the optimum bondline thickness for the samples processed by RI technique was about 5 mm. To correlate the maximum applied load, F_{max}, with the bondline thickness, t_{bl}, in the single lap shear tests, a nonlinear asymptotic regression is proposed for the samples processed by the resin infusion technique

$$F_{max} = \alpha(1 - \exp(-\beta t_{bl})) \quad (6)$$

where α and β are constants. For RI system, α and β are found to be 26.01 and 0.646, respectively. Unknown parameters, α and β, are adopted in a way to find the best regression for the results considering the standard deviation of different types of functions.

After the tests, it was observed that in all of the samples, debonding occurred in a thin layer of the concrete close to the interface which is called cohesive failure. The thickness of the fractured layer is on average 0.5 mm and slightly increases for the samples with more GFRP layers (Fig. 8). Cohesive failure mainly occurs due to the lower shear and tensile strength of the concrete in comparison with the resin. The same type of debonding was observed for the pultruded samples which were tested by the authors previously [26,34]. It indicates that for the samples which were prepared by the resin infusion process, the quality of the bond between fibres and adhesive and also between FRP and concrete was satisfactory. Therefore, samples processed by RI technique can significantly show the same pattern in terms of debonding failure mode as the commonly used processing methods, such as pultruded or wet lay-up technique. Due to the 25 mm initial unbonded zone, adopted for all of the samples, near end failure of the concrete prism was not observed after the tests.

As mentioned in the previous section, the maximum load increases with the application of a thicker bondline. However, after the optimum bondline thickness, no further increase is observed in the load carrying capacity of the joints. Results indicate that using more GFRP layers in the bondline leads to a reduction in slip at maximum load stage (Fig. 9). When the bondline thickness increases, deeper surfaces of the concrete under the FRP get involved in the interfacial stress transfer which can be observed in Fig. 8. The depth of IC debonding, attached to the FRP plates after the tests, increases for samples with 0–6 GFRP plates (Fig. 8a–d). Consequently, the slip at the maximum load stage decreases which leads to more brittle response of the joints. On the contrary, based on the experiments carried out on the lap

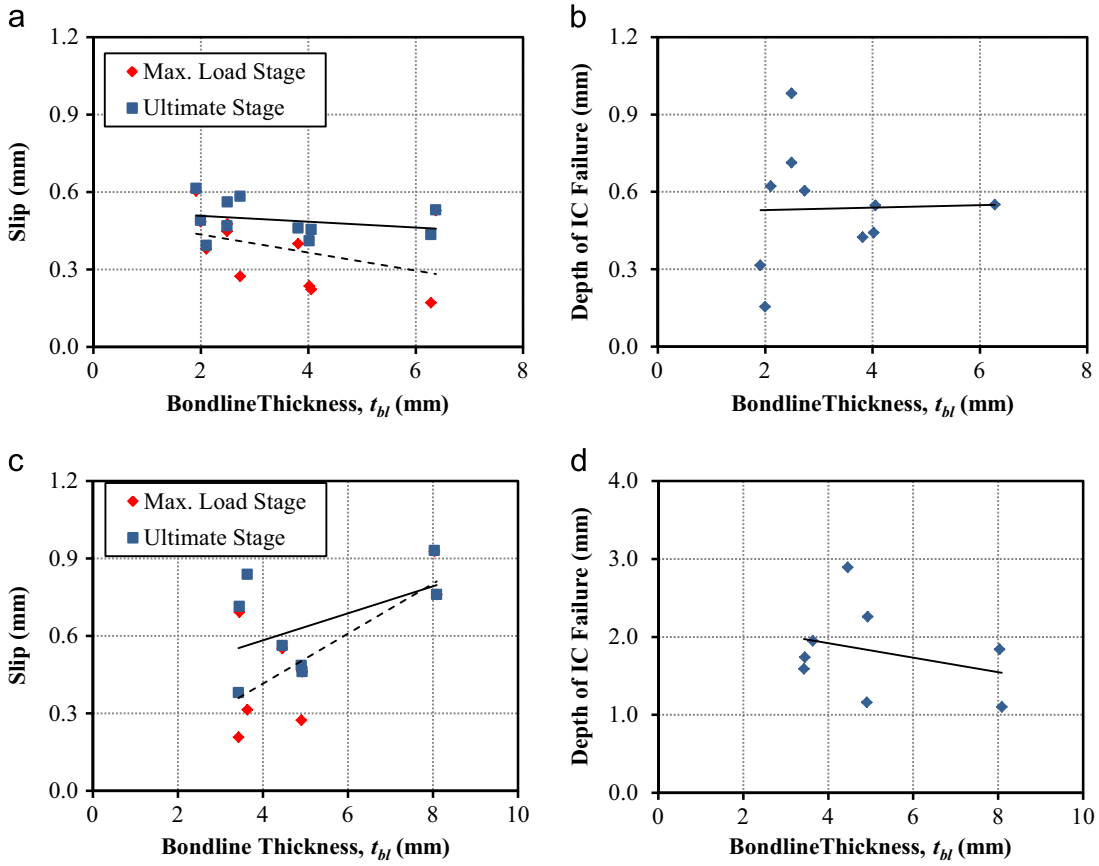

Fig. 9. Correlation between slip and depth of IC failure with the GFRP layers for (a, b) RI processed samples and (c, d) pultruded plates.

shear joints using pultruded plates by the authors [26], thicker bondline leads to higher slip and lower depth of IC debonding (Fig. 9c and d).

A new method was developed by Hadigheh et al. [26] to estimate the interfacial shear stress, τ_{int}, along the bonded length considering the applied load at the loaded end of FRP

$$\tau_{int,x} = \left(\frac{d^2 s_x}{dx^2}\right) t_{frp} E_{frp} = \frac{d\varepsilon_{frp,x}}{dx} t_{frp} E_{frp} \tag{7}$$

where t_{frp}, E_{frp} and $\varepsilon_{frp,x}$ are the FRP thickness, FRP modulus of elasticity and strain of the FRP, respectively. The local slip, s_x, at every location from the free end of the FRP, x, is the difference between the displacement of the FRP and the concrete substrate

$$s_x = u_{frp,x} - u_{c,x} \tag{8}$$

$$s_x = \int \varepsilon_{frp,x} dx - \int \varepsilon_{c,x} dx \tag{9}$$

where $u_{frp,x}$ and $u_{c,x}$ are the displacements of the FRP and concrete at any point, respectively and $\varepsilon_{c,x}$ is the strain in concrete. The local slip at every position can be derived from the strain values by integration of the strain profile along the bond length up to that position

$$s_{L-x} = s_L + \int_{L-x}^{L} \varepsilon_{frp,x} dx \tag{10}$$

where x, L and s_L are the distances relative to the free end, the FRP length, and the local slip at the loaded end, respectively. The shear stress–local slip (τ–s) profile of the samples with different bondline thicknesses for three locations along the FRP is presented in Fig. 10. According to Fig. 10a, the loaded end experiences variation in the shear–slip profile. Therefore in the analysis, the shear stress–slip curves of the inner sections, x=182.5 and 157.5 mm in which the τ–s profiles are smoother, were used rather than those at the loaded end. Based on Fig. 10(b–d), samples with 3 GFRP layers show higher maximum shear stresses.

The maximum shear stress of the samples decreases towards the free end of the FRP plate. Samples with different bondline thicknesses show the same trend in terms of the shear stress–slip curves closer to the FRP free end (Fig. 10c and d). In addition, the local slip of the sections very close to the free end (x=40 and 7.5 mm), which are not presented here, is negligible. The shear stress has the maximum value at the loaded end and decreases towards the end of the effective bond length, L_{eff}. It indicates that the effective bond length is less than 200 mm in the samples processed with RI technique which in this research is adopted to 150 mm. The same length was reported for pultruded plates in another study by Hadigheh et al. [26].

The changes of the maximum shear stress corresponding to the bondline thickness for different positions along the bonded length are shown in Fig. 11. For t_{bl}=6.377 mm, the maximum shear stress at x=197.5 mm was obtained almost 30 MPa while for the other locations, the maximum value is 7.8 MPa. Since the variance is high, this maximum shear stress is ignored and the modified graph is shown in Fig. 11b. Except for x=125 mm, the maximum shear stress increases for the bondline thickness up to 3.815 mm and drops for t_{bl}=6.377 mm. This maximum shear stress response for different bondline thicknesses can support the concept of the optimum bondline thickness which indicates that after a specific thickness, bond strength does not increase for thicker bondlines.

When the bonded length is sufficiently greater than the effective bond length, L_{eff}, the maximum transferable load, F_{max}, can be predicted by solving differential equation (Eq. (7)) based on energy criteria of the linear elastic fracture mechanics in

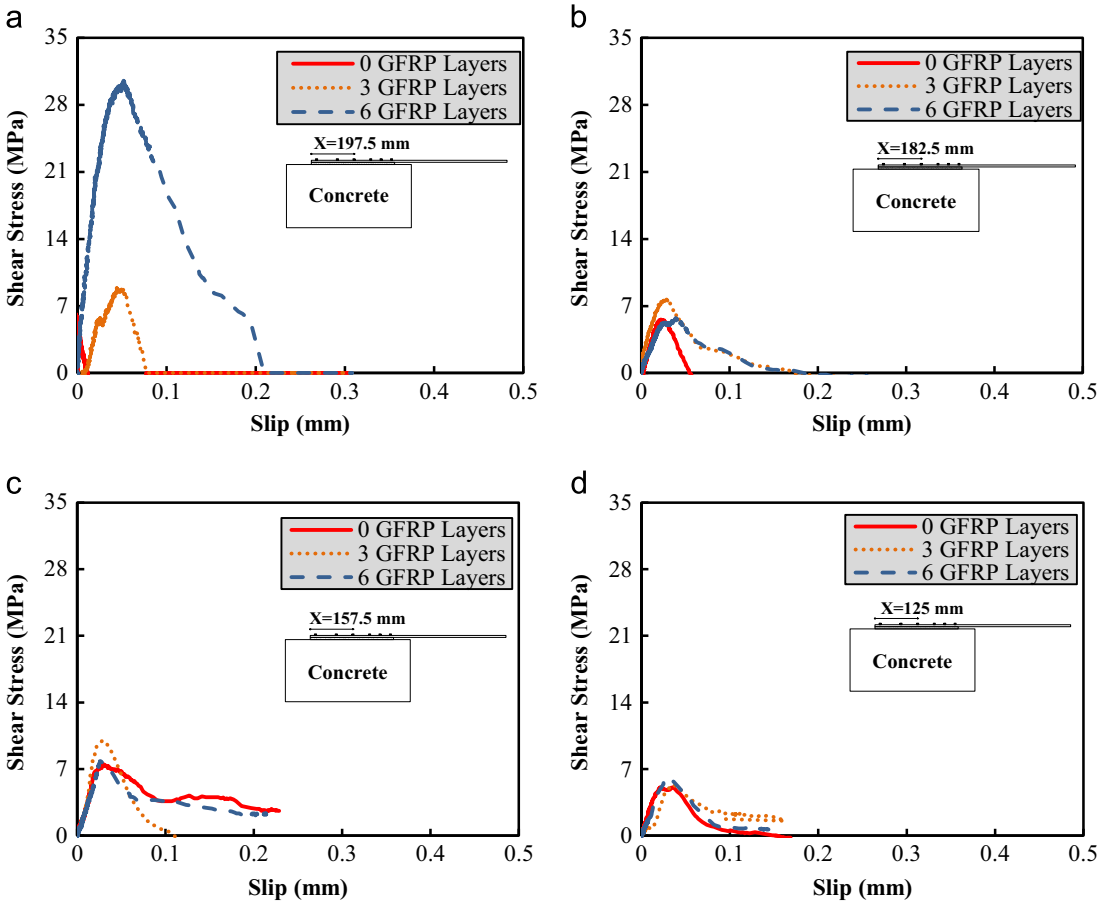

Fig. 10. Interfacial shear stress–slip profiles for the samples at different locations; (a) $x=197.5$ mm, (b) 182.5 mm, (c) 157.5 mm, and (d) 125 mm.

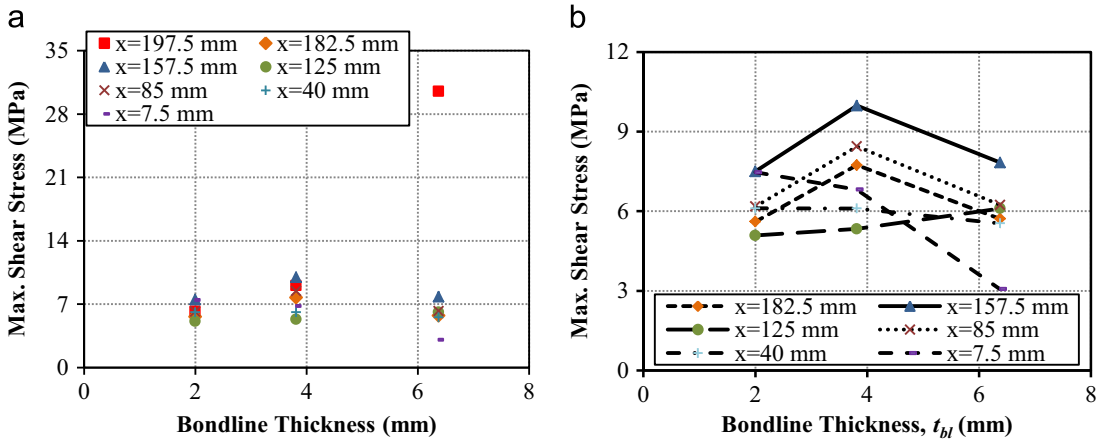

Fig. 11. Maximum shear stress along the FRP plate considering different bondline thicknesses.

conjunction with the simple beam theory

$$F_{max} = W_{frp}\sqrt{2E_{frp}t_{frp}G_F} \tag{11}$$

where W_{frp} is the FRP width and G_F is the interfacial fracture energy (antisymmetric in-plane shear mode)

$$G_F = \frac{8L_{eff}^2}{81(Et)_{ftrp}}\tau_{max}^2 \tag{12}$$

where τ_{max} is the maximum shear stress of the interface. The analytical values of F_{max} and G_F, predicted by Eqs. (11) and (12), are presented in Table 3. Results show that Eq. (11) can predict the maximum applied load with a high precision while Eq. (12) slightly overestimates the interfacial fracture energy.

6. Conclusions

The bond characteristics between RI processed FRP plates and concrete substrate were studied in this research. Experiments were carried out by the application of a new modified single lap shear test set-up which facilitates to monitor the slip between the FRP plate and substrate during the test with higher precision. During the experiments, the effect of the FRP thickness on the

Table 3
Comparison between analytical and experimental results.

Specimen ID	Analytical interfacial fracture energy, $(G_F)_{anal.}$, (N/mm)[a]	Analytical max. load, $(F_{max})_{anal.}$, (kN)[b]	G_F (anal./exp.)	F_{max} (anal./exp.)
SF-B-1.1	0.27	13.8		0.8
SF-B-1.2	0.28	13.8		0.8
SF-B-1.3	0.26	13.8	1.5	0.8
SF-B-2.1	0.46			
SF-B-2.2	0.51			
SF-B-2.4	0.47			
SF-B-3.1	0.57	23.2		0.9
SF-B-3.2	0.51	23.2		1.0
SF-B-3.3	0.43	23.2	0.9	1.1
SF-B-4.1	0.58	21.3		0.8
SF-B-4.2	0.58	21.3	1.4	0.8

[a] Calculated based on Eq. (12).
[b] Calculated based on Eq. (11).

interface behaviour was considered by variation of the bondline from 2 mm to 6 mm. In addition, the performance of the bond between concrete and RI processed plates was compared with that of the pultruded laminates.

Considering the bondline thickness, samples with thinner bondline show softer behaviour during the initial stages of loading. This response may be attributed to the surface condition of the substrate. When the bondline thickness decreases, the impact of the concrete surface condition on the interfacial behaviour increases. Therefore, thinner bondline cannot sufficiently restrain the initiated cracks at the linear stage of the load–slip response. Nonlinear analysis on the MSLS test results indicates that thicker bondline may not continuously increase the load carrying capacity and suggests the existence of the optimum bondline thickness in the adhesively bonded joints. The same behaviour was observed from the tests carried out by authors on pultruded samples and also specimens processed by the vacuum and heat.

Post-processing analysis showed that although the maximum shear stress increases with use of thicker bondlines, after a specific amount of bondline thickness the maximum shear stress drops. These phenomena support the concept of the optimum bondline thickness. Finally, a relationship was proposed to estimate the maximum applied load in single lap shear tests based on bondline thickness. Considering the type of debonding in RI processed samples, the type of failure is similar to pultruded laminates and wet lay-up systems.

Acknowledgement

The authors would like to acknowledge the financial and technical support of RMIT University and Inovas Pty Ltd. The authors would also like to thank Melbourne Testing Services Co. (MTS) for providing the equipment for the tensile testing.

References

[1] Teoh KJ, Hsiao K-T. Improved dimensional infidelity of curve-shaped VARTM composite laminates using a multi-stage curing technique – experiments and modeling. Compos Part A: Appl Sci Manuf 2011;42(7):762–71.
[2] Silva-Muñoz RA, Lopez-Anido RA. Structural health monitoring of marine composite structural joints using embedded fiber Bragg grating strain sensors. Compos Struct 2009;89(2):224–34.
[3] Dodkins AR, Shenoi RA, Hawkins GL. Design of joints and attachments in FRP ships' structures. Mar Struct 1994;7(2–5):365–98.
[4] Chalmers DW. Experience in design and production of FRP marine structures. Mar Struct 1991;4(2):93–115.
[5] Mcllhagger A, Brown D, Hill B. The development of a dielectric system for the on-line cure monitoring of the resin transfer moulding process. Compos Part A: Appl Sci Manuf 2000;31(12):1373–81.
[6] Poodts E, Minak G, Zucchelli A. Impact of sea-water on the quasi static and fatigue flexural properties of GFRP. Compos Struct 2013;97:222–30.
[7] Zainuddin S, Hosur MV, Zhou Y, Kumar A, Jeelani S. Durability study of neat/nanophased GFRP composites subjected to different environmental conditioning. Mater Sci Eng A 2010;527(13–14):3091–9.
[8] Morales G, Barrena MI, Salazar JMGD, Merino C, Rodríguez D. Conductive CNF-reinforced hybrid composites by injection moulding. Compos Struct 2010;92(6):1416–22.
[9] Deka LJ, Bartus SD, Vaidya UK. Multi-site impact response of S2-glass/epoxy composite laminates. Compos Sci Technol 2009;69(6):725–35.
[10] Böger L, Wichmann MHG, Meyer LO, Schulte K. Load and health monitoring in glass fibre reinforced composites with an electrically conductive nanocomposite epoxy matrix. Compos Sci Technol 2008;68(7–8):1886–94.
[11] Hayward JS, Harris B. The effect of vacuum assistance in resin transfer moulding. Compos Manuf 1990;1(3):161–6.
[12] Edwards KL. An overview of the technology of fibre-reinforced plastics for design purposes. Mater Des 1998;19(1–2):1–10.
[13] Kessels JFA, Jonker AS, Akkerman R. Fully flow modeling of resin infusion under flexible tooling using unstructured meshes and wet and dry compaction properties. Compos Part A: Appl Sci Manuf 2007;38(1):51–60.
[14] Correia NC, Robitaille F, Long AC, Rudd CD, Šimáček P, Advani SG. Analysis of the vacuum infusion moulding process: I. Analytical formulation. Compos Part A: Appl Sci Manuf 2005;36(12):1645–56.
[15] Williams C, Summerscales J, Grove S. Resin infusion under flexible tooling (RIFT): a review. Compos Part A: Appl Sci Manuf 1996;27(7):517–24.
[16] Zhou S, Wang Z, Zhou J, Wu X. Experimental and numerical investigation on bolted composite joint made by vacuum assisted resin injection. Compos Part B: Eng 2013;45(1):1620–8.
[17] Himmel N, Bach C. Cyclic fatigue behavior of carbon fiber reinforced vinylester resin composites manufactured by RTM and VARI. Int J Fatigue 2006;28(10):1263–9.
[18] Täljsten B, Elfgren L. Strengthening concrete beams for shear using CFRP-materials: evaluation of different application methods. Compos Part B: Eng 2000;31(2):87–96.
[19] Canning L, Hollaway L, Thorne AM. An investigation of the composite action of an FRP/concrete prismatic beam. Constr Build Mater 1999;13(8):417–26.
[20] Alampalli S, O'Connor J, Yannotti A. Design fabrication construction, and testing of an FRP superstructure. State Campus, Albany, New York: New York State Department of Transportation; 2000 12232-0869.
[21] Alampalli S, O'Connor J, Yannotti AP. Fiber reinforced polymer composites for the superstructure of a short-span rural bridge. Compos Struct 2002;58(1):21–7.
[22] Hejll A, Täljsten B, Motavalli M. Large scale hybrid FRP composite girders for use in bridge structures—theory, test and field application. Compos Part B: Eng 2005;36(8):573–85.
[23] Dagher HJ, Bannon DJ, Davids WG, Lopez-Anido RA, Nagy E, Goslin K. Bending behavior of concrete-filled tubular FRP arches for bridge structures. Constr Build Mater 2012;37:432–9.
[24] Dawood M, Ballew W, Seiter J. Enhancing the resistance of composite sandwich panels to localized forces for civil infrastructure and transportation applications. Compos Struct 2011;93(11):2983–91.
[25] Gravina RJ, Hadigheh SA, Setunge S, Kim SJ. Application of heat/resin injection in the presence of vacuum for FRP attachments on the concrete substrate. Appl Mech Mater 2013;438–439:459–66.
[26] Hadigheh SA, Gravina RJ, Setunge S. Experimental and analytical identification of interfacial bond characteristics in adhesively bonded joints. In: Proceedings of the 11th international symposium on fiber reinforced polymers for reinforced concrete structures (FRPRCS11), Guimarães, Portugal; 2013.
[27] ASTM C39/C39M-09a. Standard test method for compressive strength of cylindrical concrete specimens. West Conshohocken, PA; 2009.
[28] ASTM D3039/D3039M. Standard test method for tensile properties of polymer matrix composite materials. West Conshohocken, PA: ASTM International; 2008.
[29] Hadigheh SA, Gravina RJ, Setunge S, Kim SJ. Experimental study on the bondline behavior between concrete and FRP materials. In: From materials to structures: advancement through innovation, CRC Press; 2012. p. 505–11.
[30] Hadigheh SA, Gravina RJ, Setunge S. Shear debonding of FRP plates from concrete surface: using modified single lap shear test set-up. In: Proceedings of the 6th international composites conference (ACUN-6), Melbourne, Australia; 2012. p. 175–80.
[31] Krenchel H. Fibre reinforcement. Copenhagen: Akademisk Forlag; 1964.
[32] Gravina RJ, Hadigheh SA, Setunge S. Interfacial bond strength of resin impregnated fibre reinforced polymer laminates bonded to concrete using vacuum and heat: experimental study. Aust J Struct Eng 2014;15(2):189–201.
[33] Hadigheh SA, Gravina RJ, Setunge S. Interfacial stress distribution of FRP-to-concrete joints using advanced composite processing techniques. In: Proceedings of the 6th international conference on FRP composites in civil engineering (CICE 2012), Rome, Italy; 2012.
[34] Gravina RJ, Hadigheh SA, Setunge S. Bond and force transfer of FRP materials bonded to concrete using sitecure system. In: Proceedings of the 3rd Asia-Pacific conference on FRP in structures (APFIS 2012), Japan; 2012.